Research Square

Preprints are preliminary reports that have not undergone peer review.
They should not be considered conclusive, used to inform clinical practice,
or referenced by the media as validated information.

Effect of Particle Breakage on Strength Characteristics of Limestone Aggregate

Israa Alhani
Mazaya university college
Wael M. Albadri (wael.mahmood@alamarahuc.edu.iq)
Al-Amarah university college
Mohd Jamaludin Md Noor
MARA University of Technology: Universiti Teknologi MARA
Sin Mei LIM
National University of Singapore
Adam Alwash
Curtin University - Perth City Campus

Research Article

Keywords: limestone aggregate, particle breakage, acid rain, single-particle strength, friction angle, stress-strain curve

Posted Date: April 8th, 2022

DOI: https://doi.org/10.21203/rs.3.rs-1520672/v1

License: This work is licensed under a Creative Commons Attribution 4.0 International License.
Read Full License

Effect of Particle Breakage on Strength Characteristics of Limestone Aggregate

Israa J. Alhani

Faculty of Civil Engineering, Mazaya University College, Thi-Qar, Iraq

Wael M. Albadri (Corresponding author)
Al-Amarah University College, Misan, Iraq

E-mail: wael.mahmood@alamarahuc.edu.iq

Mohd Jamaludin Md Noor

Faculty of Civil Engineering, MARA University of Technology UiTM, 40450, Shah Alam, Selangor, Malaysia

Sin Mei LIM

Faculty of Engineering, Department of Civil and Environmental Engineering, National University of Singapore, 21 Lower Kent Ridge Rd, Singapore 109077

Adam Alwash

Curtin University GPO Box U1987 Perth, Western Australia, Australia Perth WA 6102 Australia

Abstract

Particle breakage is one of the issues that significantly affect the strength characteristics of aggregate. In this paper, the strength of pre-crushed limestone aggregate was evaluated through investigating the friction angle, stress-strain behaviour, and single-particle strength. The particle breakage phenomenon was studied for samples prepared at different conditions, including non-soaked samples, water-soaked samples, and acid-soaked samples. The purpose of preparing the samples at different conditions was to simulate the effect of environmental factors on the breakage behaviour of limestone aggregate. The test program of this paper consists of two phases of triaxial tests: the initial shearing and second shearing. The test results showed remarkable variations among the samples since limestone aggregate tended to experience more particle breakage after being soaked in water and acid solution. Also, the volume change results

exhibited an increase in dilation as the breakage index increases. The test results of this study presented the importance of considering the role of environmental factors in evaluating the particle breakage of limestone aggregate.

Keywords: limestone aggregate; particle breakage; acid rain; single-particle strength; friction angle; stress-strain curve

1. Introduction

The gradation of aggregate plays a vital role in providing the required particles-interlocking and determining the packing order of the particles. It also affects the shear strength, stiffness, load-carrying capacity and the permanent deformation characteristics [1-5].

However, the gradation of aggregate may change progressively and significantly with the occurrence of particle breakage, that takes place when the particles subjected to external stresses that exceed the limits of the particle strength [6, 7]. Therefore, for a better understanding of the strength and stress-strain behaviour of aggregate, it is important to incorporate the breakage index, which defines the degree of particle breakage, into the mathematical models that adequately represent the strength behaviour of aggregate [8-12].

The particle breakage can be presented as disintegrative fracture, attrition, abrasion, or particle splitting. In general, particle breakage produces fine particles and small fragments when the neighbouring particles are sheared under specific stresses [13].

Therefore, the shape of particles may change after applying static and cyclic loading [14, 15].

The amount of particle breakage is governed by several factors such as particle angularity, particle size distribution, initial void ratio and confining pressure [16]. The environmental factors (such as erosion and floods) were also regarded as factors to influence the particle breakage [14, 17]. Mun and McCartney [16] stated that particle mineralogy and hardness are the most significant factors controlling the amount of breakage.

Aggregate in the field, such that exists in the road base and subbase, subjected to normal (clean) rain and acid rain. The normal rain and floods may increase the potential of particle breakage since the water reduces the hardness of the particles. This fact was highlighted by Miura and Yamanouchi [18], who observed that soil particles crack more easily at higher water content. However, the effect of water on the long-term performance of aggregate was investigated through numerous studies [19-21].

On the other hand, acid rain may increase the potential of particle breakage upon loading. The structural and chemical characteristics of limestone particles impair as a result of the dissolution of mineral components, mainly carbonate, when it is exposed to acid rain [22, 23]. Also, Corvo et al. [24] stressed that the main reason of limestone particles to be potentially affected by the surrounding environment was mainly due to the highly porous matrix that may range between 15% to 20% (or much higher at 45%). Therefore, the water and acid have straightforward access to the porous system of the limestone particles.

This paper aims to evaluate the strength of limestone aggregate that experienced particle breakage. More attention was given to investigate the influence of water and acid on the particle breakage of limestone aggregate.

1.2 Test material

1.2.1 Sample collection and preparation

Limestone boulders were obtained from a quarry located at Simpang Pulai, Perak, Malaysia. These big boulders of diameters ranging from 100 to 400 mm were broken into smaller fragments by using a breaker machine. The samples were further broken down by using a rock crusher machine. During the crushing process, fine-grained and dust materials were inevitably produced. Therefore, the crushed stones were washed thoroughly to remove these fugitive dust. The washed sample was then oven-dried for 24 hours at 105°C temperature and thereafter sieved to obtain the required gradation. The targeted test material was those passing from sieve size of 14 mm and retained on sieve size of 3.35 mm.

1.2.2 Physical and chemical properties

Physical and chemical tests were conducted to define the physical and chemical properties of the original test material. The physical properties of the test material were defined in accordance with the British Standard (BS 1377: l990). The test material was classified as poorly graded gravels, GP, based on British Soil Classification System (BS 5930: 1981). Table 1 and 2 summarised the physical properties and the chemical composition of limestone, respectively.

94 In this paper, the X-ray diffraction (XRD) test was performed to characterise the
95 crystalline materials of limestone particles by identifying XRD peaks which are produced
96 through constructive interference of a monochromatic beam of X-ray scattered at specific
97 angles from lattice planes in the sample. The test was performed after setting the kV and
98 mA to 40 kV and 30 mA, respectively, and the maximum number of counts within
99 500,000 counts, while the scan-axis was set to 2θ range. The X-rays intensities were
100 plotted as a function of the scattering angle, and thus, the material structure was
101 identified. The result obtained from the XRD test, that is shown in Fig. 1, indicated the
102 presence of one major and seven minor peaks of minerals forming the structure of the
103 limestone particles. The peaks involved calcite, lime, dolomite, and aragonite. The major
104 peak was identified as calcite and had an intensity of 25,000 counts.
105

106 **1.3 Research methodology**

107 The test materials were prepared at different conditions to simulate various
108 environmental effects on limestone aggregate. The original test material was prepared at
109 different conditions before conducting the initial shearing test. The samples were divided
110 into three groups; each group represent a particular sample preparation condition. Table 3
111 summarises the preparation conditions and the testing purpose. The acidic solution used
112 in this paper was prepared by adding 1 ml of sulfuric acid (H2SO4) to 30L of distilled
113 water to ensure an acidic solution with pH = 4.
114 This paper is following the testing approach established by Yu [6] to evaluate the effect
115 of particle breakage on soil strength. The test program consists of two phases of triaxial
116 tests; the initial shearing and the second shearing. The purpose of the initial shearing

117 phase is to produce pre-crushed aggregate, while the purpose of the second shearing is to
118 evaluate the strength of the aggregate that previously experienced particle breakage (pre-
119 crushed aggregate).
120 The initial shearing was conducted by using the triaxial test at confining stress of 1000
121 kPa, the shearing rate was maintained as 0.03 mm/min. During the initial shearing phase,
122 the tests were ceased at various axial strain values to evaluate the particle breakage at
123 different stages during shearing. Trial tests were conducted at first to identify the axial
124 strain values corresponding to the shearing stages (strain hardening, peak stage, and strain
125 softening) at the given confining stress. Therefore, the tests were ceased at axial strain
126 values of 0.07, 0.15 and 0.25 to represent the three shearing stages.
127 After finishing the initial shearing for all samples, sieve tests were carried out to measure
128 the amount of particle breakage and calculate the breakage index for all samples.
129 All pre-crushed samples were then subjected to second shearing which was conducted at
130 relatively low effective stress (50 kPa) to minimise the potential of further particle
131 breakage in the second shearing, as was recommended by Yu [6]. Consequently, the
132 variations in stress-strain results of the second shearing can be attributed to the effect of
133 particle breakage only. In order to confirm the absence of further particle breakage in the
134 second shearing, the shape of stress-strain curves was always observed. According to
135 Bishop [25], the sign for the occurrence of particle breakage is the flattened stress-strain
136 curve. In other words, the specimens that show peak stress did not experience particle
137 breakage. Therefore, the specimens that showed flattened stress-strain curve will not be
138 included or further discussed in this paper.
139

1.3.1 Identifying the breakage index

In order to quantify the amount of particle breakage, the particle breakage index proposed by Marsal [26] was considered in this study. The method involved measuring the change in grain size distribution curves that resulted from particle breakage through conducting sieve tests before and after the initial shearing. From the recorded changes in particles size distribution, the difference in the percentage retained on each sieve size ($\Delta Wk = Wki - Wkf$) is computed, where (Wki) represent the percentage retained on sieve size 'k' before the test and (Wkf) is the percentage retained on the same sieve size after the test. Marsal [26] noticed that some of these differences were positive and some were negative. Theoretically, the sum of all positive values of (ΔWk) must be equal to the sum of all negative values. Marsal [26] defined the breakage index (Bg) as the sum of the positive values of (ΔWk) expressed as a percentage. The breakage index (Bg) has a lower limit of zero which indicates no particle breakage and has a theoretical upper limit of unity 100% which represents all particles broken to sizes below the smallest sieve size used.

1.4 Results and analysis

1.4.1 Initial shearing

All samples were initially sheared using the CD triaxial tests at confining pressure of 1000 kPa, and the results were expressed through the stress-strain curves after analysing the data obtained from the load cell and the attached LVDT. Taking σ_1 and σ_3 as the major and minor effective principal stresses, the deviator stress can be calculated as $\sigma_1 - \sigma_3$. Fig. 2 illustrate the stress-strain curves and volume change results for all the groups of samples that were tested at different axial strains (0.07, 0.15, and 0.25).

163 The results shown in Figs. 2(a-c) indicate that the deviator stress was increasing with the
164 increase of axial strain until it reaches a constant value with a continuous increase of
165 axial strain. The highest values of the deviator stress were recorded from samples of
166 group A, whereas the lowest values were recorded from acid-soaked samples (group C).
167 The results indicated the effect of acid and water in producing greater amounts of crushed
168 particles that contributed to decreasing the deviator stresses in the groups mentioned
169 above.
170 As the deviator stress increases, the particles move to a denser packing by moving into
171 empty void spaces until an interlocking condition is achieved. At this stage, the volume
172 change behaviour is exhibiting a continuous specimen volume decrease. However, there
173 are two possible scenarios after the full particle interlocking attained at which the
174 specimen volume can either be increasing or decreasing. In both cases, the specimen
175 height is shortened due to the advancement of the load cell piston. In the first case, the
176 height shortened while the specimen dilates, which resulted in an overall volume increase
177 and thus, the deviator stress decreased. In the second case, as the specimen's height
178 became shorter, the overall volume decreased without any radial expansion. In this case,
179 there had to be particle breakage otherwise dilation would have occurred since the
180 particles were already interlocking. Therefore, the compression behaviour of samples
181 from group A, B and C is obviously attributed to the particle breakage because, at high
182 confining pressure, the particles were crushed in their position rather than being dilated.
183 According to the results shown in Figs. 2(d-f), the highest compression was observed
184 from specimens of group C because these specimens underwent the most considerable

185 particle breakage compared with the specimens from other groups (more details will be
186 provided in the next subsection).
187 The objective of this phase of testing was to produce pre-crushed aggregate obtained
188 from samples prepared at different conditions and sheared until certain axial strains. The
189 objective was achieved, and the pre-crushed aggregate specimens were all kept in
190 separated and labelled plastic bags to be used later for further tests.
191

192 **1.4.2 Sieve test of the pre-crushed aggregate**

193 The quantity of crushed particles was measured for all specimens after finishing the
194 initial shearing by calculating the breakage index based on the particle size distribution
195 curves before and after the initial shearing. According to the results shown in Fig. 3, the
196 specimens of group C demonstrated the greatest particle breakage among the other
197 groups. A general observation can be made that the retained weight on all sieves smaller
198 than 3.35 mm was increased after the initial shearing, and most of the particles retained
199 on sieve size of 10 mm were broken into smaller fragments. Alaei and Mahboubi [27]
200 stated that large particles are more likely to crush because such particles exposed to
201 higher contact forces, and therefore, these particles demonstrate more defects and faults
202 than the smaller particles.
203 The changes in the key parameters of the particle-size distributions due to the particle
204 breakage are summarised in Table 4.
205 Based on the results shown in Table 4, the particle breakage of specimens within the
206 same group was seen to be increasing as the axial strain increases. However, the breakage
207 index was slightly reduced at the axial strain of 0.25. A similar trend of results was also

reported by Indraratna and Salim [2]. Also, the coefficient of uniformity, Cu, was increasing as the particle breakage increases; this behaviour was also reported by numerous studies [28, 29].

The remarkable increase in the breakage index for the water-soaked and acid-soaked specimens is demonstrating the effect of water and acid in impairing the structure of particles that became prone to break upon loading.

According to Fukumoto [9], when the particle breakage occurs, the physical and mechanical properties of the soil undergo significant changes. However, the results in Figures 4(a-c) and in Table 4, are indicating the fact that the pre-crushed aggregate exhibited different proportions of particle sizes that were not existed in the original sample (without particle breakage). Thus, the minimum and maximum void ratios that were determined for the original aggregate are no longer valid for the pre-crushed aggregate. Therefore, tests were conducted to calculate the minimum and maximum void ratios for all pre-crushed specimens.

On the other hand, in order to evaluate the stress-strain curves of all specimens consistently and accurately, the initial void ratio was maintained constant for all the second shearing tests through maintaining a constant mass of soil for all the tests so that the volume of soil can be constant for all tests, as expressed in Eq. 1

$$V_s = \frac{M_s}{G_s \rho_w} \tag{1}$$

Then, the volume of voids can be determined using Eq. 2

$$V_v = V - V_s \tag{2}$$

Thus, the void ratio can be found by using Eq. 3

$$e = \frac{V_v}{V_s} \tag{3}$$

Where V_s = volume of soil particles; M_s = mass of soil particles; G_s = specific gravity; ρ_w = water density; V = total volume of specimen; V_v = volume of voids; and e = void ratio. However, the minimum and maximum void ratios vary among the specimens with different proportions of crushed particles. Specimens that experienced great particle breakage demonstrated low minimum and maximum void ratios since the produced fine particles tended to fill the voids within the soil matrix. Therefore, despite the fact that the specimens in the second shearing tests were prepared at a constant initial void ratio, they were at different relative densities, D_r, since the latter calculated based on the minimum and maximum void ratios, as well as the initial void ratio, as shown in Eq. 4

$$D_r = \frac{e_{\max} - e}{e_{\max} - e_{\min}} \tag{4}$$

Where D_r = relative density; $e_{\min}$ = minimum void ratio; and $e_{\max}$ = maximum void ratio. Table 5 illustrates the minimum and maximum void ratios and the corresponding relative densities for all samples with different breakage indices. According to the results shown in Table 5, the maximum and minimum void ratio decreases as the crushed particles increases. By maintaining the initial void ratio constant, the relative density decreases as the particle breakage increase due to the reported decrease in the maximum and minimum void ratio. Salgado et al. [30] conducted a study to assess the shear strength of sand at different fine contents, and therefore, the samples were prepared at different relative densities. A similar approach was followed in this paper.

1.4.3 Second shearing

Stress-strain curves and volume change results of the second shearing tests that were conducted at confining pressure of 50 kPa are shown in Figs 4(a-f). Figures 4(a-c) are presenting the effect of the particle breakage on the stress-strain behaviour of all pre-crushed specimens. The results indicated a remarkable decrease of maximum deviator stress for the specimens of groups C and B as the breakage index increases. In contrast, no significant decrease was reported from specimens of group A. The maximum deviator stress values were ranging from 380 kPa to 365 kPa, 361 kPa to 328 kPa, and 353 kPa to 312 kPa for the specimens of groups A, B and C, respectively. The stress-strain curves of specimens from group A are almost consistent because the quantity of crushed particles in these specimens could not contribute to decreasing in the deviator stress.

For demonstrating the role of particle breakage in decreasing the maximum deviator stresses, reduction percentage of maximum deviator stress of all specimens was calculated by referring to that of the original sample (Bg = 0), as presented in Table 6. The maximum reduction percentage was 19% which reported from the specimen of group C with breakage index of 38.27.

The crushing of the sharp corners of the particles, that contribute to the strength of the angular particles, could be the reason behind the reported reduction of deviator stress. The angular particles gain the strength from the high particles-interlocking upon loading. After the particle breakage, the shape of particles could be converted to rounded and semi-rounded particles, and consequently, the friction angle is reduced. The angle of

friction of the pre-crushed specimens was calculated based on the effective principal stresses at failure, as presented in Eq. 5:

$$\sin\phi' = \frac{(\sigma_1')_f - (\sigma_3')_f}{(\sigma_1')_f + (\sigma_3')_f} \quad (5)$$

Where ϕ' = effective friction angle; σ_1' = major principle effective stress; and σ_3' = minor principle effective stress. Table 7 is showing the variation of friction angles for the pre-crushed specimens. It is clearly shown that there is a very minimal decrease in the friction angle for the specimens of group A (52.5 to 51.93°). While the specimens of group C exhibit a maximum drop of the friction angle (52.5° to 50°) with the increase of breakage index. The results of friction angles and the stress-strain curves of pre-crushed aggregate are evidence of the effect of particle breakage on reducing the strength of aggregate, as well as demonstrating the influence of the acidic solution and the water in increasing the particle breakage. The obtained results are consistent with those obtained by Yu [6].

Figures 4(d-f) illustrated the volume change behaviour of pre-crushed specimens. All specimens showed compression behaviour until the full particle-interlocking was attained, then all specimens were dilated. The specimens were compressed as the deviator stress increases and peaked at the maximum compression where the full particle-interlocking was attained. With the continuous increase of loading, the specimens were dilated, and the deviator stress was decreasing.

The results are showing that the dilation increases as the particle breakage increase, and therefore, the maximum dilation was reported from specimens of group C which experienced the most significant particle breakage among the specimens of other groups.

An observation can be made that the deviator stress decreases with the increasing of dilation and breakage index, and these three parameters are strongly linked.

1.4.5 Effect of Water and Acid on Particle Breakage

In order to investigate the effect of water and acid on limestone particle strength, single-particle crushing tests were conducted on particles from each sample (original aggregate, water-soaked aggregate and acid-soaked aggregate).

Results of the tests are presented in force-displacement space, as illustrated in Fig. 5. The results showed several peaks and the displacement value corresponding to the peak points were varied among the specimens. The original aggregate showed the highest peak (P1) at relatively low displacement, and it was dropped down significantly implying stiff crushing. With continuous loading, the force was slightly increased in another peak point (P2) and dropped down again. Almost similar behaviour was observed in the water-soaked particle but with lower ranges of peak points (P3 and P4). However, the acid-soaked particle did not show well-defined peak points. The force was increased gradually, and the maximum peak (P6) was attained at relatively high displacement, implying brittle crushing. The results indicated the effect of water and acid in reducing the particle strength and explaining the reason why the soaked samples showed greater particle breakage than the original samples. Previous studies such as [31, 32] have also reported a similar trend of results and agreed that because of dissolving the calcium carbonate of the limestone in an acid-contaminated area, the strength of limestone particles is significantly affected.

According to the chemical test results, the limestone particles consist almost entirely of calcite, which is the most stable polymorph of calcium carbonate ($CaCO_3$) as was stated by Meng and Li and Corvo et al. [22, 24]. Calcite carbonate bonds are the source of the particle strength due to its high cementation effect [22, 33-35]. Subjecting the limestone aggregate to an acidic solution, such that in the acidic rain, will inevitably lead to the destruction of the carbonate cementation in limestone particles. According to Meng and Li [22], the cementation bonds are destroyed upon the removal of large amounts of carbonate and causing the particle strength to decrease. Therefore, the particle breakage was the maximum in the acid-soaked specimens. Similarly, Beck et al. [36] stated that water affects the particle structure and can be responsible for its deterioration. In general, the porous matrix of the limestone particles is providing straightforward access of water and acid to the particle structure and weakening the particle strength.

1.5 Conclusion

The following conclusions are drawn from the findings of this study:

1. The results of sieve tests showed significant particle breakage in the samples soaked in water and acid, whereas the non-soaked samples exhibited less particle breakage.
2. The particle breakage plays a vital role in decreasing the deviator stress and increasing the dilation of pre-crushed aggregate. The results showed that the more particle breakage, the less value of maximum deviator stress and more dilation.

3. The friction angle showed a remarkable decrease as the breakage index increases. However, the friction angle of the non-soaked samples was almost constant due to the low range of breakage indices.
4. The results of single-particle crushing tests suggested that the water and acid are reducing the particle strength significantly. Therefore, the particle breakage for the samples immersed in water and acid presented greater breakage indices.

Declarations

- **Funding:** This research did not receive any specific grant from funding agencies in the public, commercial, or not-for-profit sectors

- **Conflicts of interest/Competing interests:** The authors declare that they have no conflict of interest.
- **Availability of data and material:** The datasets generated during and/or analysed during the current study are not publicly available due to the technical or time limitations but are available from the corresponding author on reasonable request.

References

1. Bilodeau, J. P., G. Dore, and P. Pierre: Erosion susceptibility of granular pavement materials. Int. J. Pavement Eng. 8(1), 55-66 (2007)
2. Indraratna, B. and W. Salim: Modelling of particle breakage of coarse aggregates incorporating strength and dilatancy. P. I. Civil Eng-Geotec. 155(4), 243-252 (2002)
3. Alhani, I. J., bin Md Noor, M. J., Al-Bared, M. A. M., Harahap, I. S. H., and Albadri, W. M.: Mechanical response of saturated and unsaturated gravels of different sizes in drained triaxial testing. Acta Geotechnica. 1(19), (2020).

4. Alsaadi, K. A., and Aljorany, A. N.: Experimental and Numerical Study on the Pullout Resistance of a Single and Group of Granular Pile Anchor (GPA) in Soft Soils. Modern Applications of Geotechnical Engineering and Construction. 133-145, (2021).
5. Alhani, I. J., Noor, M. J. M., and Albadri, W. M.: Membrane penetration effects on shear strength and volume change of soil during triaxial test. AIP Conference Proceedings (Vol. 2020, No. 1, p. 020008). AIP Publishing LLC (2018, October).
6. Yu, F.: Particle breakage and the drained shear behavior of sands. Int. J. Geomech. 17(8), 04017041 (2017)
7. Peng, Yu, Ding, X., Xiao, Y., Deng, X., and Deng, W.: Detailed amount of particle breakage in multi-sized coral sands under impact loading. Eur. J. Environ. Civ. Eng. 1(10), (2020).
8. Hardin, B.O.: Crushing of soil particles. J. Geotech. Eng. 111(10), 1177-1192 (1985)
9. Fukumoto, T.: Particle breakage characteristics of granular soils. Soils Found. 32(1), 26-40 (1992)
10. Chen, Q., Indraratna, B., Carter, J.P. and Nimbalkar, S.: Isotropic–kinematic hardening model for coarse granular soils capturing particle breakage and cyclic loading under triaxial stress space. Can. Geotech. J. 53(4), 646-658 (2016)
11. Raisianzadeh, J., S. Mohammadi, and A.A. Mirghasemi: Micromechanical study of particle breakage in 2D angular rockfill media using combined DEM and XFEM. Granul. Matter. 21(3), 48 (2019)
12. Guo, W., Huang, Y., Fourie, A., and Wu, Y.: Mathematical model revealing the evolution of particle breakage and particle-size distribution for rockfill during triaxial shearing. Eur. J. Environ. Civ. Eng. 1(16), (2019).
13. Valdes, J.R. and E. Koprulu: Characterization of fines produced by sand crushing. J. Geotech. Geoenviron. Eng. 133(12), 1626-1630 (2007).
14. Alhani, I. J., Albadri, W. M., Noor, M. J. M., Wong, S. Y., and Wong, K. Y.: Technique to Avoid Membrane Punching During Triaxial Test of Crushed Aggregate. Transportation Infrastructure Geotechnology. 1-12 (2020).

15. Indraratna, B. and W. Salim: Mechanics of ballasted rail tracks: a geotechnical perspective. CRC Press. (2005)
16. Mun, W. and J.S. McCartney: Roles of particle breakage and drainage in the isotropic compression of sand to high pressures. J. Geotech. Geoenviron. Eng. 143(10), 04017071 (2017)
17. Wu, M. and J. Wang: A DEM investigation on crushing of sand particles containing intrinsic flaws. Soils Found. (2020)
18. Miura, N. and T. Yamanouchi: Effect of water on the behavior of a quartz-rich sand under high stresses. Soils Found. 15(4), 23-34 (1975)
19. Zhang, Y., Ishikawa, T., Tokoro, T. and Nishimura, T.: Influences of degree of saturation and strain rate on strength characteristics of unsaturated granular subbase course material. Transp. Geotech. 1(2), 74-89 (2014)
20. Kuttah, D. and H. Arvidsson: Effect of groundwater table rising on the performance of a Swedish-designed gravel road. Transp. Geotech. 11, 82-96 (2017)
21. Albadri, W. M., Noor, M. J. M., & Alhani, I. J.: The relationship between the shear strength and water retention curve of unsaturated sand at different hydraulic phases. Acta Geotechnica, 1-15, (2021).
22. Meng, J. and X. A. Li: Effects of carbonate on the structure and properties of loess and the corresponding mechanism: an experimental study of the Malan loess, Xi'an area, China. Bull. Eng. Geol. Environ. 78(7), 4965-4976 (2019)
23. Eyssautier C., S., Marin, B., Thomachot-Schneider, C., Fronteau, G., Schneider, A., Gibeaux, S. and Vazquez, P.: Simulation of acid rain weathering effect on natural and artificial carbonate stones. Environ. Earth Sci. 75(9), 748 (2016)
24. Corvo, F., Reyes, J., Valdes, C., Villaseñor, F., Cuesta, O., Aguilar, D. and Quintana, P.: Influence of air pollution and humidity on limestone materials degradation in historical buildings located in cities under tropical coastal climates. Water Air Soil Pollut. 205(1-4), 359 (2010)
25. Bishop: The strength of soils as engineering materials. Rankine Lecture, Geotechnique, . 16(2), 91-130 (1966)

26. Marsal, R.J.: Large-scale testing of rockfill materials. J. Soil Mech. Found. Div. 93(2), 27-43 (1967)
27. Alaei, E. and A. Mahboubi: A discrete model for simulating shear strength and deformation behaviour of rockfill material, considering the particle breakage phenomenon. Granul. Matter. 14(6), 707-717 (2012)
28. Wang, T., Liu, S., Feng, Y. and Yu, J.: Compaction characteristics and minimum void ratio prediction model for gap-graded soil-rock mixture. Appl. Sci. 8(12), 2584 (2018)
29. Indraratna, B., Q.D. Sun, and S. Nimbalkar: Observed and predicted behaviour of rail ballast under monotonic loading capturing particle breakage. Can. Geotech. J. 52(1), 73-86 (2015)
30. Salgado, R., P. Bandini, and A. Karim: Shear strength and stiffness of silty sand. J. Geotech. Geoenviron. Eng. 126(5), 451-462 (2000)
31. Bakhshipour, Z., Asadi, A., Huat, B.B., Sridharan, A. and Kawasaki, S.: Effect of acid rain on geotechnical properties of residual soils. Soils Found. 56(6), 1008-1020 (2016)
32. Gratchev, I. and I. Towhata: Compressibility of natural soils subjected to long-term acidic contamination. Environ. Earth Sci. 64(1), 193-200 (2011)
33. Canakci, H., W. Sidik, and I.H. Kilic: Effect of bacterial calcium carbonate precipitation on compressibility and shear strength of organic soil. Soils Found. 55(5), 1211-1221 (2015)
34. Pedrotti, M. and A. Tarantino: Effective stresses for unsaturated states stemming from clay microstructure. Geomech. Energy Envir. 15, 74-84 (2018)
35. Sharma, A. and R. Ramkrishnan: Study on effect of Microbial Induced Calcite Precipitates on strength of fine grained soils. Perspect. Sci. 8, 198-202 (2016)
36. Beck, K., Al-Mukhtar, M., Rozenbaum, O. and Rautureau, M.: Characterization, water transfer properties and deterioration in tuffeau: building material in the Loire valley—France. Build. Environ. 38(9-10), 1151-1162 (2003)

Table 1
The physical properties of limestone aggregate

Parameter	Value
Max dry density (ton/m^3)	1.695
Min dry density (ton/m^3)	1.434
Specific gravity	2.7
Relative density (%)	58
Max. void ratio	0.882
Min void ratio	0.592
Initial void ratio	0.713
C_u	1.94
C_c	0.95
$D6_0$ (mm)	8.05
D_{50} (mm)	7.18
D_{30} (mm)	5.63
D_{10} (mm)	4.14

Table 2
The chemical composition of limestone aggregate

Chemical component	Value
Na2O, (%)	0.332
MgO, (%)	2.109
Al2O3, (%)	0.681
SiO2, (%)	0.712
P2O5, (%)	0.020
SO3, (%)	0.051
K2O, (%)	0.068
CaO, (%)	58.562
TiO2, (%)	0.123
MnO, (%)	1.050
Fe2O3, (%)	36.291

Table 3
Sample preparation conditions for the initial shearing

Group name	Sample preparation condition	Purpose of the test
Group A	Non-soaked	To investigate the breakage at normal condition
Group B	Soaked 90 days in the water	To simulate the effect of clean rain
Group C	Soaked 90 days in an acidic solution (pH=4)	To simulate the effect of acid rain

Table 4
Gradation parameters and the breakage indices of the pre-crushed aggregate

Group name	Axial strain	Weight of particles < 3 mm (gm)	D_{10} (mm)	D_{30} (mm)	D_{50} (mm)	D_{60} (mm)	C_u	C_c	Bg
A	0.07	73	3.884	5.273	6.601	7.595	1.96	0.94	7.55861
	0.15	151	3.619	5.000	6.140	7.149	1.98	0.97	12.93452
	0.25	183	3.523	4.853	6.000	6.875	1.99	0.97	15.56184
B	0.07	251	3.280	4.873	6.077	6.926	2.11	1.05	14.47049
	0.15	550	0.979	3.949	5.428	6.098	6.23	2.61	23.24171
	0.25	700	0.548	3.479	4.988	5.609	10.23	3.94	31.40663
C	0.07	400	1.144	4.430	5.804	6.540	5.72	2.62	18.06791
	0.15	750	0.435	3.298	4.960	5.576	12.82	4.48	32.65966
	0.25	899	0.398	2.482	4.452	5.198	13.06	2.98	38.27809

Table 5
Maximum and minimum void ratios and the corresponding relative densities of pre-crushed aggregate

Group name	Bg	e_{min}	e_{max}	Relative density
A	7.55	0.568	0.834	0.45
	12.93	0.546	0.807	0.36
	15.56	0.522	0.792	0.29
B	14.47	0.548	0.823	0.40
	23.24	0.509	0.781	0.25
	31.40	0.500	0.751	0.15
C	18.06	0.526	0.807	0.33
	32.65	0.489	0.766	0.19
	38.27	0.432	0.737	0.07

Table 6
The reduction percentage of deviator stress corresponding to the breakage indices

Group name	Axial strain (%)	Breakage index (%)	Reduction of deviator stress due to breakage (%)
Group A	0.07	7.55	2.33
	0.15	12.93	3.89
	0.25	15.56	4.67
Group B	0.07	14.47	7
	0.15	23.24	12.2
	0.25	31.4	14.8
Group C	0.07	18.06	9.09
	0.15	32.65	15.58
	0.25	38.27	18.96

Table 7
Variations of friction angles corresponding to the breakage indices

Group name	Axial strain	Breakage index	Friction angle
Original aggregate	-	0	52.5
A	0.07	7.558	52.218
A	0.15	12.934	52.032
A	0.25	15.561	51.933
B	0.07	14.470	51.622
B	0.15	23.241	50.927
B	0.25	31.406	50.599

C	0.07	18.067	51.369
C	0.15	32.659	50.508
C	0.25	38.278	50.022

List of Figures

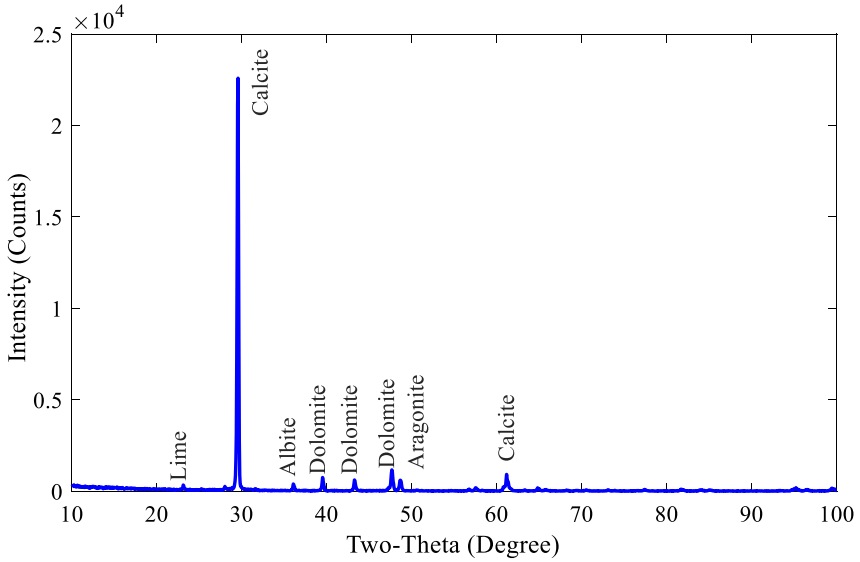

Fig. 1. Results of XRD test for the test material

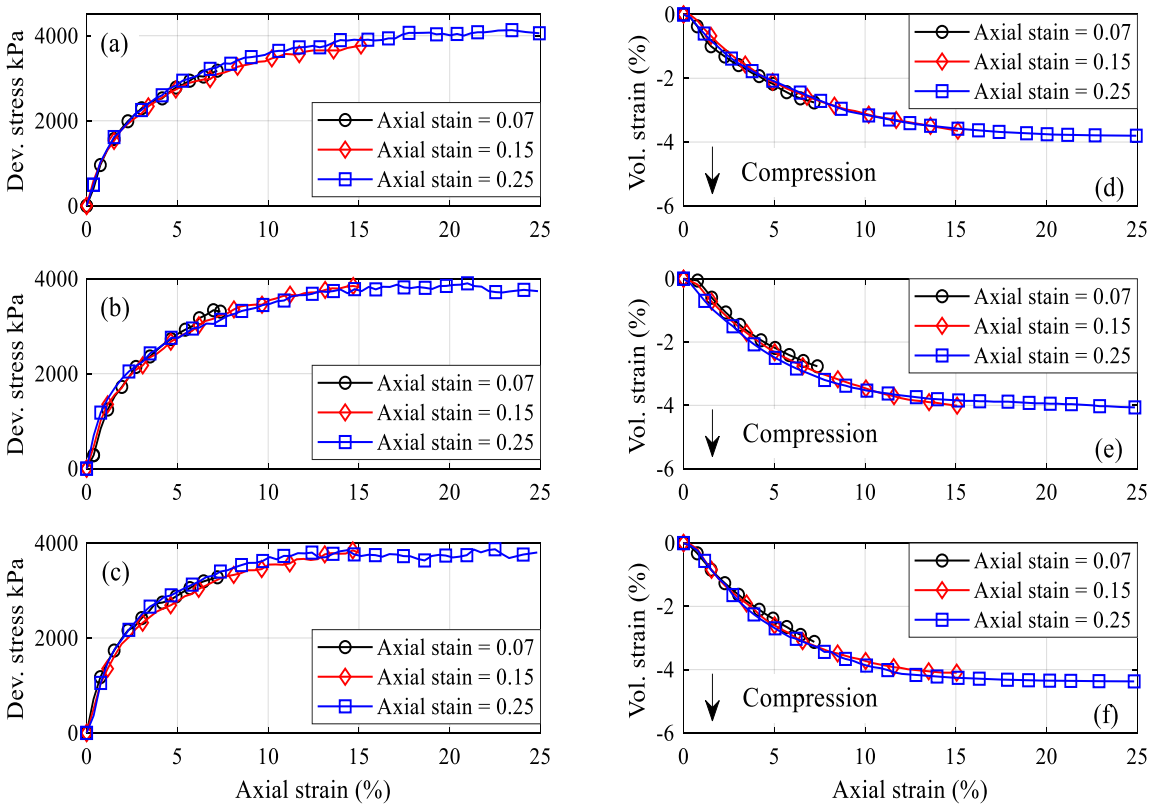

Fig. 2. Stress-strain and volume change results of the initial shearing phase; (a), (b), and (c), are the stress-strain curves of specimens from groups (A), (B) and (C), respectively; (d), (e), and (f) are the volume change results of specimens from groups (A), (B) and (C), respectively

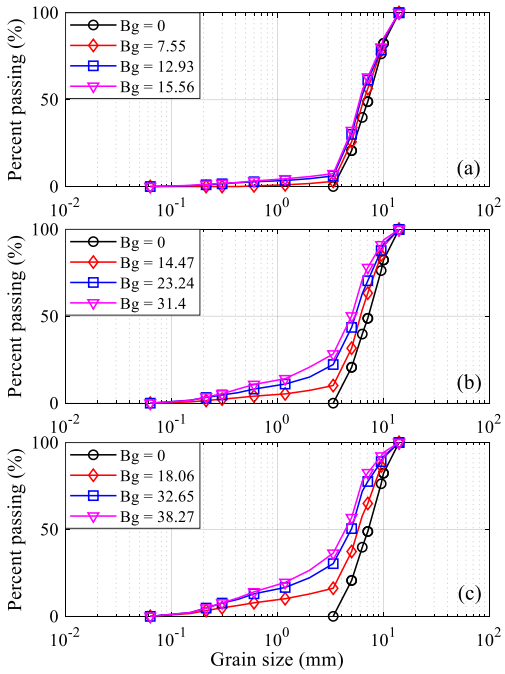

518

519 **Fig. 3.** Particle size distribution curves of pre-crushed aggregate of groups A, B and C

520

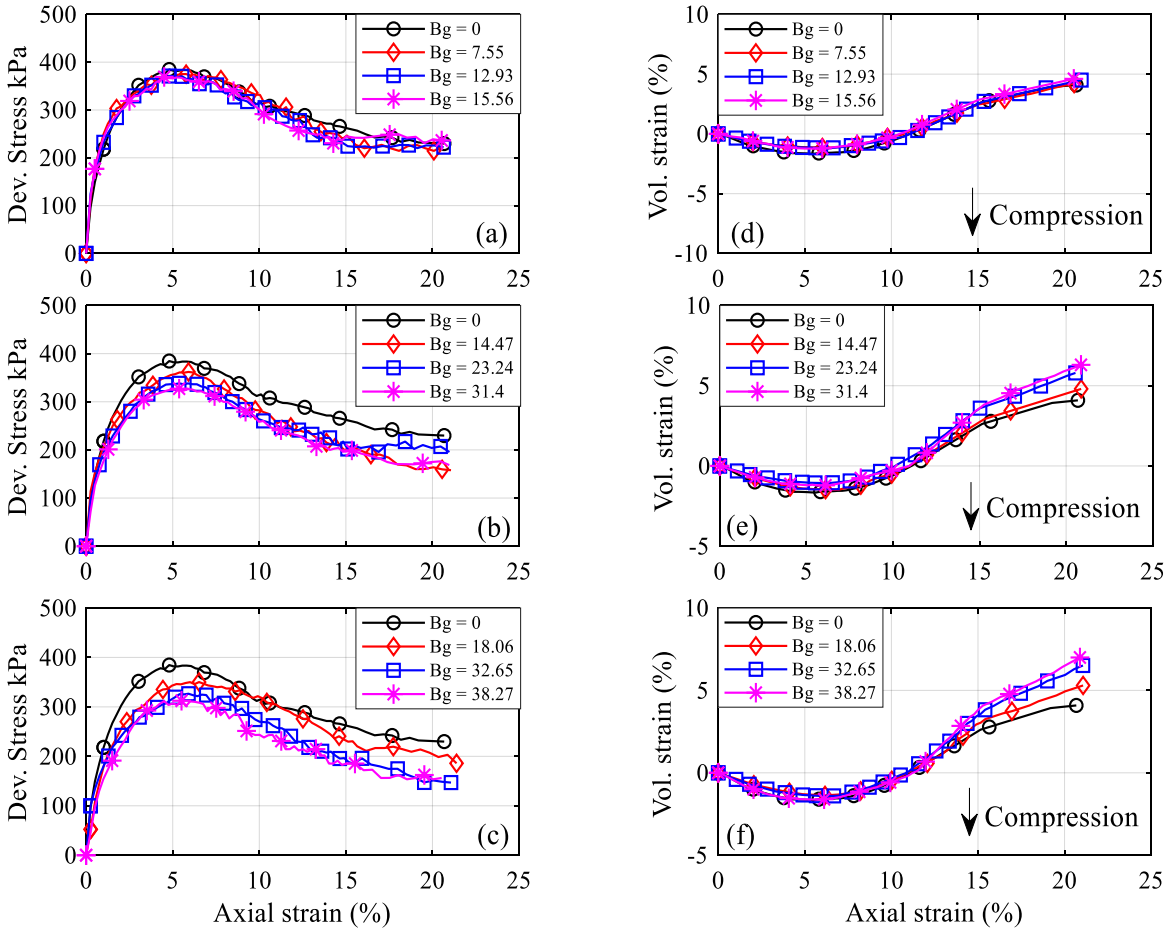

Fig. 4. Stress-strain and volume change results of the second shearing phase; (a), (b), and (c), are the stress-strain curves of specimens from groups (A), (B) and (C), respectively; (d), (e), and (f) are the volume change results of specimens from groups (A), (B) and (C), respectively

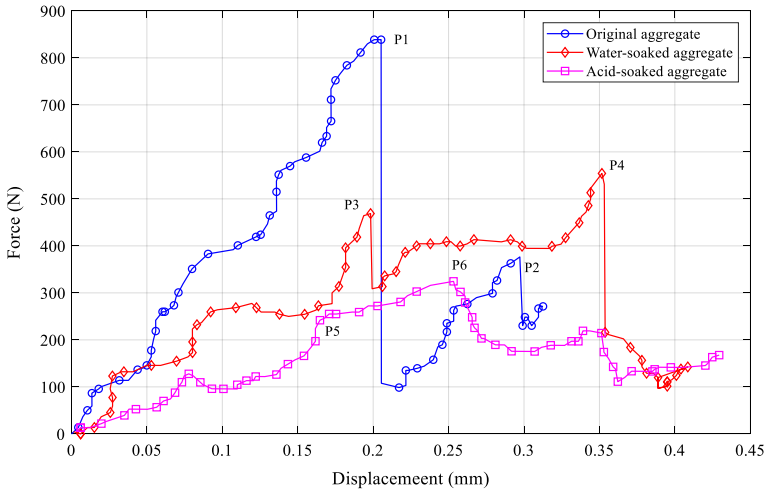

Fig. 5. Results of single-particle crushing test for limestone particles